**J. Cent. South Univ.** (XXXX) XX: 1−16
**DOI:** https://doi.org/10.1007/s11771-025-5869-7

Springer

# Comparative mechanisms of Cr(VI) adsorption on biosynthetically derived Iron-minerals

ZHANG Ke(章可)[1], ZENG Xiang-feng(曾祥峰)[2], WANG Jun(汪俊)[3],
GAN Min(甘敏)[1]*, ZHU Jian-yu(朱建裕)[1, 3], HE Qiang(何强)[3],
Hazen Terry C.[3], LIU Jun-wu(刘军武)[4], FANG Ying-chun(方迎春)[4]

1. School of Minerals Processing and Bioengineering, Key Laboratory of Biometallury of Ministry of Education, Central South University, Changsha 410083, China;
2. Key Laboratory of Pollution Ecology and Environment Engineering, Institute of Applied Ecology, Chinese Academy of Sciences, Shenyang 110016, China;
3. Department of Civil and Environmental Engineering, The University of Tennessee, Knoxville, Tennessee, USA;
4. Hunan Engineering Technology Research Center for Treatment and Recycling of Heavy Pollution Industrial Wastewater, Changsha 410083, China



**Graphic abstract:**

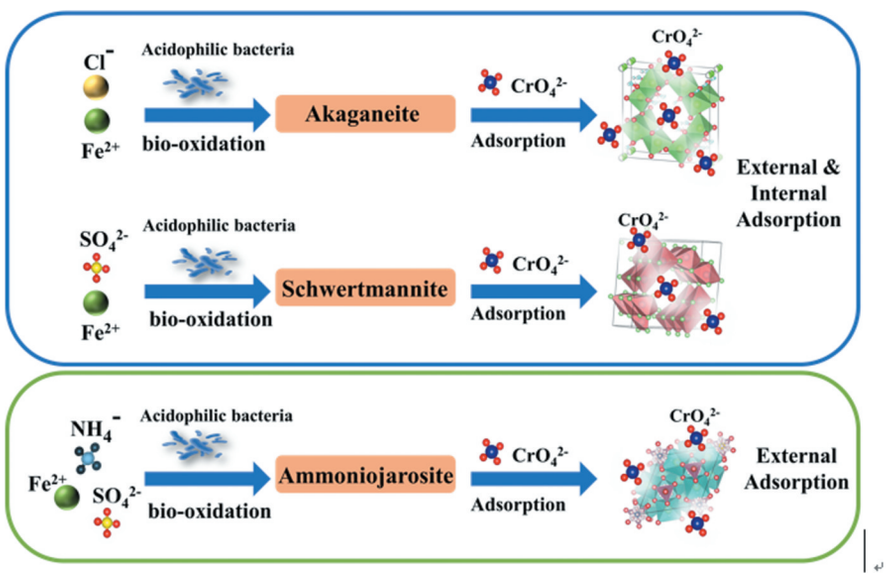


**Foundation item:** Project(42277256) supported by the National Natural Science Foundation of China; Project(HBKT-2021011) supported by the Hunan Province Environmental Protection Research Program; Project(HBKT-2021014) supported by the Hunan Province Environmental Protection Research Program; Project(CDSKY-2023-05) supported by the Scientific research project hunan provincial urban geological survey and monitoring Institute.
**Received date:** 2023-10-13; **Accepted date:** 2024-08-12
**Corresponding author:** GAN Min, PhD, Professor; E-mail: ganmin0803@sina. com; ZHU Jian-yu, PhD, Professor; E-mail: zhujy@csu. edu. cn; ORCID: https://orcid.org/0000-0003-0905-3814

**Abstract:** In this study, Schwertmannite, Akaganéite and Ammoniojarosite were biosynthesized by different bacteria and characterized. Our results showed that bacteria are critical in mediating the mineral formation process: the morphology, crystallinity, grain size and specific surface area of each mineral varied upon different bacteria and culturing conditions. In addition, the formed minerals' elemental composition and group disparity lead to different morphology, crystallinity and subsequent adsorption performance. In particular, adsorption difference existed in iron minerals biosynthesized by different bacteria. The maximal adsorption capacity of Akaganéite, Schwertmannite and Ammoniojarosite were 26.6 mg/g, 17.5 mg/g and 3.90 mg/g respectively. Our results also suggest that Cr(VI) adsorption on iron-minerals involves hydrogen bonding, electrostatic interaction, and ligand exchange. The adsorption only occurred on the surface of Ammoniojarosite, while for Akaganéite and Schwertmannite, the tunnel structure greatly facilitated the adsorption process and improved adsorption capacity. Thus, we conclude that the molecular structure is the primary determining factor for adsorption performance. Collectively, our results can provide useful information in selecting suitable bacteria for synthesizing heavy-metal scavenging minerals according to different environmental conditions.

**Key words:** Iron-secondary minerals; Biosynthesize; Biomineralization; Cr(VI) adsorption; Heavy-metal scavenging minerals

**Cite this article as:** ZHANG Ke, ZENG Xiang-feng, WANG Jun, GAN Min, ZHU Jian-yu, HE Qiang, Hazen Terry C., LIU Jun-wu, FANG Ying-chun. Comparative mechanisms of Cr(VI) adsorption on biosynthetically derived Iron-minerals [J]. Journal of Central South University, XXXX, XX(XX): 1−16. DOI: https://doi.org/10.1007/s11771-025-5869-7.

## 1 Introduction

Chromium (Cr) is a typical contaminant whose primary existing forms are Cr(III) and Cr(VI) in the environment, and the toxicity and migration of the former are significantly weaker than the latter [1]. The World Health Organization (WHO) limits drinking water's safe Cr(VI) to 0.05 mg/L [2]. Therefore, reducing Cr(VI) to Cr(III) and adsorbing chromium are the most effective ways to treat chromium pollution in the environment [3]. Moreover, due to the environment's complexity, the adsorption method has more application advantages than the reduction method [4, 5]. Therefore, optimizing adsorption materials is an effective way to control environmental chromium pollution.

Natural iron-minerals are an aristocracy of chromium adsorption materials with high adsorption performance and no secondary pollution, in which the iron-secondary minerals are particularly striking [6]. Among iron-secondary minerals, Schwertmannite, Akaganéite, and Ammoniojarosite have been extensively investigated for their efficient chromium scavenging capability through adsorption, coprecipitation, and structural incorporation [7, 8]. These iron oxyhydroxides frequently occur as very small crystals with large surface areas covered with functional groups, which allow the adsorption of chromium [9, 10]. Schwertmannite is a poorly crystalline Fe(III) - oxyhydroxysulfate with a variable composition, typically represented as $Fe_8O_8(OH)_{8-2x}(SO_4)_x$ (x=1 to 1.75) [11, 12]. With a large reactive surface, Schwertmannite can scavenge chromium and other trace elements [7, 13]. Meanwhile, Schwertmannite has a tunnel structure similar to Akaganéite ($\beta$ -FeOOH). Sulfate connects the Fe atoms lining adjacent walls of the tunnels and serves as a specifically adsorbed surface component [11, 14]. Akaganéite ($\beta$ -FeOOH; $FeO(OH)_{1-x}Cl_x$) has a tetragonal structure consisting of double chains of edge-shared octahedra that share corners with adjacent chains to form channels running parallel to the *c*-axis [9, 15]. The tunnel structure makes akaganéite a promising material as catalyst, electrode, and ion exchanger, especially in the treatment of chromium and arsenate contaminated water [9, 16, 17]. Ammoniojarosite may form diffusion barriers on mineral surfaces which can inhibit bioleaching [18]. The ammonium group in ammoniojarosite has two different orientations with equal probability. Hydronium commonly substitutes into jarosite group mineral structures [19].

Iron-secondary minerals are widespread in acid mine drainage (AMD) and acid sulfate soil (ASS) environments, mainly formed through the iron/sulfur redox pathway mediated by acidophilic bacteria [20, 21]. Thus, biosynthesis is an important pathway for the formation of iron-secondary

minerals. In order to improve the adsorption capacity of secondary minerals for heavy metals, the influence of physical and chemical factors, including pH, temperature, formation time, growth medium, and monovalent cation composition on formed materials were tested [22-25], while the influence of the involved bacteria was ignored. Significantly, the effect of bacteria with different physio-biochemical characteristics to the adsorption capacity and behavior of the formed minerals is unclear. In this study, four acidophilic bacteria strains (*Acidithioobacillus ferrooxidans*, *Leptospirillum ferrooxidans*, *Leptospirillum ferriphilum* YSK, and *Sulfobacillus thermosulfidooxidans*) with excellent acid resistance and heavy metal toxicity resistance, were used in the mineral biosynthesis. *A. ferrooxidans* can obtain energy from oxidation of reduced sulphur or ferrous ion, whose optimal growth temperature is 30 ℃ [26]. *Leptospirillum*-like species are the dominant iron-oxidizing bacteria in biooxidation of pyrite and related ores; they are gram-negative, obligately chemolithotrophic, vibrio- or spiral-shaped, and able to use ferrous iron as their sole electron source [27]. The optimal growth temperature for *L. ferrooxidans* and *L. ferriphilum YSK* are 30 and 45 ℃ respectively. *S. thermosulfidooxidans* is gram-positive, endospore forming, moderately thermophilic acidophilic bacteria (45 ℃) that obtain energy by oxidizing ferrous iron, elemental sulfur and sul fi de minerals in the presence of yeast extract [28].

Bacteria not only oxidize ferrous ion but also dominate the biomineralization process. Different bacteria have varied energy choice, ferrous oxidation ability, optimal temperature, extracellular polymeric substance and metabolite, which could affect the nature of formed materials as well [29, 30]. Moreover, the formed material could migrate, enrich, transform and form secondary minerals under precise control or be induced by the groups on bacteria surface or metabolites [31]. However, no systematic studies have examined the effects of bacteria on the formation of secondary minerals and their corresponding mineralogical properties, which can provide useful information on the behaviors of heavy metals in natural environments and is critical for improved application potential. In this present study, the role of bacteria in the biosynthesis of iron oxyhydroxide, the relationship between the molecular structure of formed iron oxyhydroxides and their chromium adsorption capacity are systematically explored. In addition, the kinetic, capacity and mechanism of chromium adsorption by biosynthesized Schwertmannite, Akaganéite and Ammoniojarosite were systematically investigated and compared to explain the mechanism of significant adsorption differences existed in different iron minerals.

## 2 Material and methods

### 2.1 Microorganism, Medium, and Strain domestication

Four acidophilic strains, *A. ferrooxidans* (30 ℃), *L. ferrooxidans* (30 ℃), *L. ferriphilum YSK* (45 ℃) and *S. thermosulfidooxidans* (45 ℃) were obtained from the Key Laboratory of Biometallurgy of Ministry of Education, China. Strains were grown in 9 K medium ($(NH_4)_2SO_4$ 3 g/L, KCl 0.1 g/L, $K_2HPO_4$ 0.5 g/L, $MgSO_4·7H_2O$ 0.5 g/L, $Ca(NO_3)_2$ 0.01 g/L) at 180 r/min and their specific optimal temperatures. Additional 0.02% yeast extract were added when growing *S. thermosulfidooxidans*. The medium was adjusted to pH 2.0 and autoclaved for 20 min at 121 ℃. Since the presence of excessive $Cl^-$, $NH_4^+$ or $Fe^{3+}$ could inhibit ferrous oxidation and growth of the bacteria [9, 31, 32], bacteria acclimation to $FeCl_2.4H_2O$, $FeCl_2·4H_2O$ and $(NH_4)_2Fe(SO_4)_2·6H_2O$ was conducted. Each strain was first cultured with initial concentration of 50 g/L $FeSO_4·7H_2O$, 20 g/L $FeCl_2·4H_2O$, and 50 g/L $(NH_4)_2Fe(SO_4)_2·6H_2O$ respectively. Then the concentration of the substrate gradually increased to acclimate the bacteria until the concentration reached 150, 59.6, and 150 g/L respectively. Acclimated bacteria were cultivated for 2 more generations until $Fe^{2+}$ oxidation rate was stable.

### 2.2 Sample preparation

Acclimated bacteria were harvested at the end of exponential phase (about four days). Cultures were first filtered by 0.45 μm filter paper to remove the precipitate. Then the filtrate was centrifuged at 12000 r/min for 20 min to harvest the cells. Cells were washed twice and resuspended in distilled water. Then each strain cultured with different substrate was added into 200 mL double distilled

water (pH 2.0) containing only 30g $FeSO_4 \cdot 7H_2O$, 11.92g $FeCl_2 \cdot 4H_2O$, and 30g $(NH_4)_2Fe(SO_4)_2 \cdot 6H_2O$ respectively. The cell density in these cultures were adjusted to $1.0 \times 10^8$ cell/mL, determined by microscopic counting prior to incubation. Under these conditions, the bacteria cannot proliferate but still possess ferrous oxidation capability. By the seventh day of incubation, the precipitate was collected with 0.45 μm filter paper through filtration, washed twice with distilled water and then dried at room temperature.

### 2.3 Cr(VI) adsorption experiment procedures

Adsorption experiments were conducted in 50 mL centrifuge tubes with Cr(VI) concentration (potassium dichromate) at 50 mg/L consisting of 0.01 mol/L $NaNO_3$ as background electrolyte. The tubes were added with 0.1g adsorbent and 20 mL pH 7.5 potassium dichromate solutions correspondingly. Then tubes were incubated for 240 min at 180 r/min, 30 ℃. For each tube, a total of 12 supernatant samples (200 μl each) were taken from 5 min to 240 min. Cr(VI) concentration in the supernatant was detected by spectrophotometer after 5 min following the 1,5-diphenyl-carbazide method. Adsorption isotherm batch experiments were conducted over a range of Cr(VI) concentrations from 5 to 250 mg/L. All centrifuge tubes were shaken for 240 min.

### 2.4 Analytical methods

Scanning electron microscope (SEM) analyses were performed with a JSM-6360LV instrument operated at 15 kV accelerating voltage. Energy dispersive spectrum (EDS) analysis were applied to the samples to quantitatively identify the major elements with rough estimates of composition based on relative peak intensities. X-Ray diffraction analysis was conducted with CuKα radiation (40 kV/250 mA) in a RINT2000 vertical goniometer. Samples were scanned from 5° to 80° with a step increment at 0.02° and 4 s counting time. The FT-IR spectra were taken on a Nicolet Nexus670 Fourier Transform spectrometer at a resolution of 4 $cm^{-1}$ using a KBr beamsplitter, a DTGS detector with KBr window, and a sample shuttle for the transmittance measurements. The background was taken on a disk made from 400 mg KBr. XANES analyses of the Cr-K edges and the Fe-K edges were performed in transmission mode at the BL14W1 XAFS beam line at the Shanghai Synchrotron Radiation Facility (SSRF). Data were analyzed using the Athena program.

The experimental data were fitted with kinetics models containing Pseudo 1st order, pseudo 2nd order, and intra-diffusion particle models.

$$\ln\left(q_e - q_t\right) = \ln q_e - k_1 t \tag{1}$$

$$\frac{t}{q_t} = \frac{1}{k_2 q_e^2} + \frac{t}{q_e} \tag{2}$$

$$\mathrm{h} = k_2 q_e^2 \tag{3}$$

$$q_t = k_i t^{0.5} + c \tag{4}$$

where $q_e$ and $q_t$ are the amount (mg/g) of adsorbed Cr(VI) on materials at equilibrium and at time t, respectively. $k_1$ is the fi rst order rate constant ($min^{-1}$). $k_2$ (g/(mg·min)) is the rate constant of pseudo-second-order, h (mg/(g·min)) is the initial sorption rate. *ki* is the intraparticle diffusion rate constant (mg/(g $min^{0.5}$)), which can be calculated from the slop of the linear plots of $q_t$ versus $t^{0.5}$.

The batch experimental data were fitted by the Langmuir and Freundlich isotherm models represented mathematically as follows.

$$q_e = q_m K_L C_e / \left(1 + K_L C_e\right) \tag{5}$$

$$q_e = K_F C_e^{1/n} \tag{6}$$

where $q_e$ is the amount of Cr(VI) adsorbed on materials in different concentration; $q_m$ is the saturated adsorption capacity; $K_L$, a constant of the Langmuir isotherm and $C_e$ is the equilibrium Cr(VI) concentration remained in the solution; $K_F$ is Freundlich constant, which indicates the relative adsorption capacity of the adsorbent; 1/n is the heterogeneity factor and is known as Freundlich coefficient.

## 3 Results and discussion

### 3.1 Characterization of biosynthesized Iron-minerals

We constructed secondary minerals synthesizing systems using different acidophilic bacteria and detected the variation in pH and ORP, which reflected the dynamic change process of

precipitate formation (Figure S1). The rising trend of pH value observed in the early stage can be attributed to the acid-consuming Fe(II) oxidation process. The subsequent dropping trend is due to the Fe(III) hydrolysis and precipitation. However, the pH in the Akaganéite formation system mediated *A. ferrooxidans* and *L. ferrooxidans* is inconsistent with others. The ORP values display a steady uptrend, which illustrates the effective oxidation of ferrous ions. These changes indicate that different bacteria mediate similar iron oxidation processes, but the oxidation rate may differ, leading to the distinction in synthetic precipitation.

The SEM images and corresponding EDS data of the precipitate samples are presented in Figures 1 and S2. Sh-Af(30) and Sh-Lf(30) showed similar structures; both of the precipitates were spherical aggregates and covered by "pincushions". This type of loose structure insures high surface area of the precipitate. Surface structure of Sh-Lf(45) was much more regular. Irregular cubic existed in Sh-St (45), which could be caused by the higher culture temperature and greater ferrous oxidation ability, as both lead to a faster growth of the precipitate and

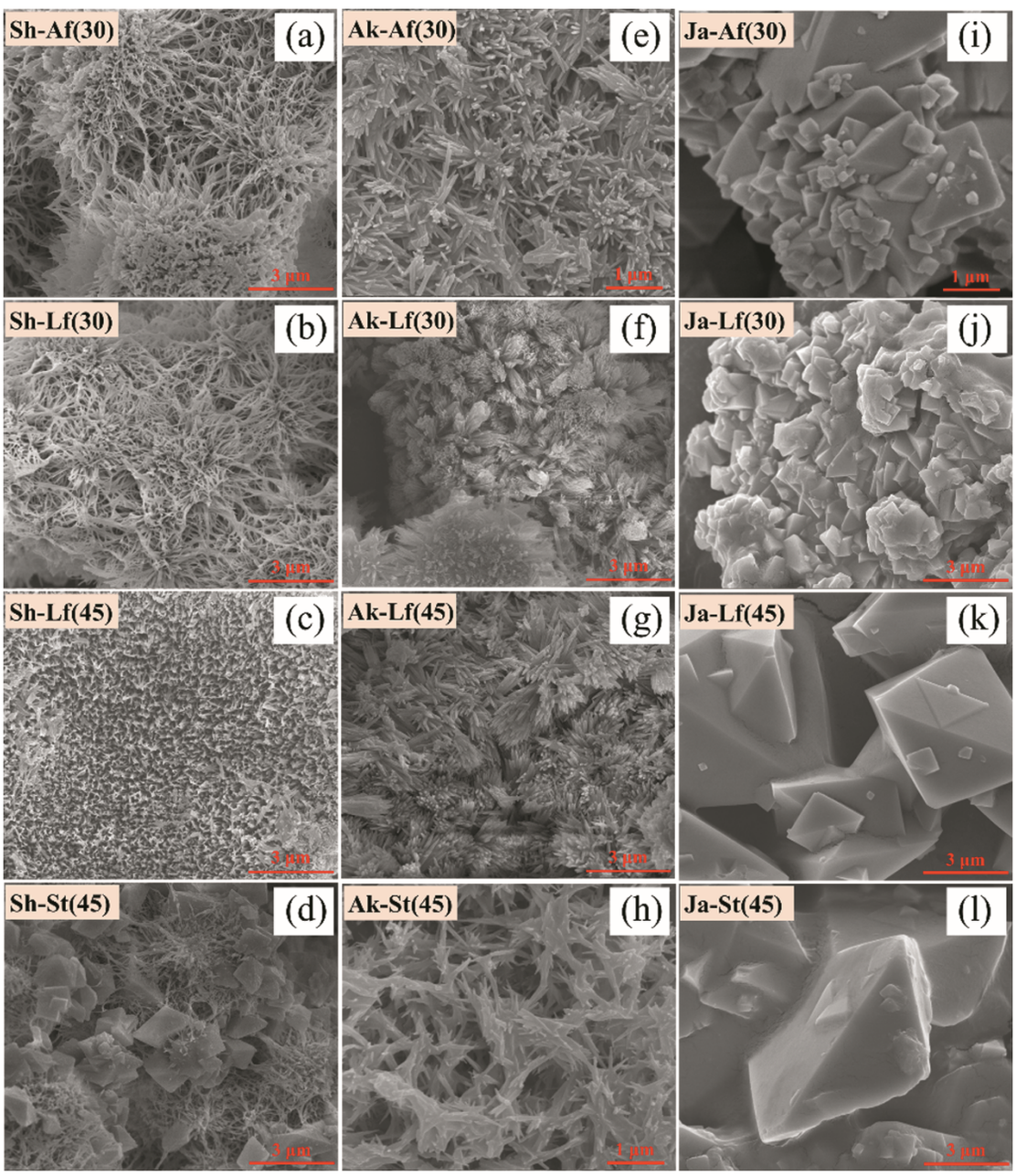


**Figure 1** The SEM images of the precipitate. Schwertmannite (a – d), Akaganéite (e – h) and Ammoniojarosite (i – l) biosynthesized by *A. ferrooxidans* (30 ℃ ), *L. ferrooxidans* (30 ℃ ), *L. ferriphilum YSK* (45 ℃ ), and *S. thermosulfidooxidans* (45 ℃) respectively

inhibit the formation of the hierarchy structure [31]. Akaganéite formed by different bacteria all presented as rod shaped crystal. Sample Ak-Lf(30) and Ak-Lf(45) showed as aggregated clusters. Ak-St (45) was smaller and longer than the others and presented as needle crystal. All four samples of Ammoniojarosite were cubic shaped while the size of Ja-Lf(45) and Ja-St(45) were more angular and bigger which may also be the result of faster precipitate growth.

Furthermore, EDS analysis revealed the specific composition of the precipitates (Table S1 and Figure S2). Schwertmannite is generally described as the chemical formula $Fe_8O_8(OH)_{8-2x}(SO_4)_x$, in which X is determined by Fe/S molar ratio [33]. The compositional formula of each precipitate produced in our study was consistent with prior study except for Sh-St(45), which was smaller than 4.3, a value usually considered as the lower limit [9, 33]. The chemical formula of Akaganéite can be summarized as $Fe_8O_8(OH)_{8-x}Cl_x$. Although differences in ferric, chloride and oxygen content between materials are not significant, diversity in shape, size, and crystal size still presented, which difference may be rooted in bacteria. As to the inner structure of Akaganéite, the tunnel is partly occupied by $Cl^-$ which is essential for its stability [34]. This tunnel position was replaced by $SO_4^{2-}$ instead of $Cl^-$ in analogous Schwertmannite and caused the difference in elemental composition, color and crystallinity [35]. Since report on chemical structure of Ammoniojarosite is not available yet, here we refer Ammoniojarosite as $Fe_8O_8(OH)_{(8+y-2x)}(NH_4)_y(SO_4)_x$ (the relative value $x$, $y$ depended on mole ratio of Fe/S and Fe/N). As shown in Table 1, the ferric content of Ammoniojarosite was lower than that of Schwertmannite and Akaganéite, which could be an important factor causing the difference in its structure and adsorption performance. The chemical form of Ja-Lf(45) and Ja-St(45) can be summarized as $Fe_8O_8(OH)_{3.01}(NH_4)_{3.14}(SO_4)_{4.06}$ and $Fe_8O_8(OH)_{0.76}(NH4)_{3.76}(SO_4)_{5.50}$ respectively. Compared to Ja-Af (30) and Ja-Lf(30) ($Fe_8O_8(OH)_{4.85}(NH_4)_{5.62}(SO_4)_{4.38}$, $Fe_8O_8(OH)_{4.55}(NH_4)_{6.31}(SO_4)_{4.88}$), Ja-Lf(45) and Ja-St (45) have much lower content of —OH, —$NH_4$, which may contribute to their bigger crystal structure.

XRD patterns (Figure 2(a)) of Schwertmannite formed in the pure $FeSO_4$ system are quite similar; no single, sharp and well recognizable peaks were observed, except the precipitate formed by *L. ferriphilum YSK* (45 ℃ ) and *S. thermosulfidooxidans* (45 ℃ ), which had better crystallinity due to the higher formation temperature and heterogeneity of bacteria. Schwertmannite belongs to non-crystal substances, so there is no specific data on grain size. Patterns of Akaganéite indicated a lower crystalline compared with previous reports [9]. This difference may be the result of different substrate compositions since only pure $FeCl_2$ with no other monovalent cation existed in the formation system. XRD pattern and its corresponding peak number (Figures 2(b), (c) and Table S1 XRD peak) suggest that Ammoniojarosite (peak numbers 13, 16, 19, 18) had a much better crystallinity than Akaganéite (peak numbers 6, 2, 4, 2). XRD peaks of Ammoniojarosite were sharp and well recognizable, and the grain size was greater than that of others (390, 411, 694, 499 nm vs. 381, 179, 358, 167 nm).

The above results indicate that bacteria affect biosynthesized iron minerals' atomic composition, crystallinity and molecular structure, which may affect their adsorption performance. Thus, a series of relevant experiments were carried out to verify this speculation.

### 3.2 Cr(VI) adsorption capacity of biosynthesized Iron-minerals

The adsorption capacity of Schwertmannite, Akaganéite and Ammoniojarosite formed by *A. ferrooxidans*, *L. ferrooxidans*, *L. ferriphilum* YSK, and *S. thermosulfidooxidans* is presented in Figure 3. The average adsorption capacity of Akaganéite, Schwertmannite, and Ammoniojarosite was 25.2, 13.8, and 4.10 mg/g respectively, which are tightly related with the nature of the materials that Akaganéite, Schwertmannite have tunnel structure while Ammoniojarosite has crystal structure without tunnel structure. In addition, it's worth noting that the absorption performance of the same type of biosynthesized mineral varied when produced by different bacteria. Schwertmannite, Ammoniojarosite formed by *L. f*(30) (15.7, 4.37 mg/g) exhibited the highest adsorption capacity compared with *A. f* (14.9, 4.22 mg/g), *L. f*(45) (13.4, 3.95 mg/g), *S. t* (11.3, 3.86 mg/g). In contrast,

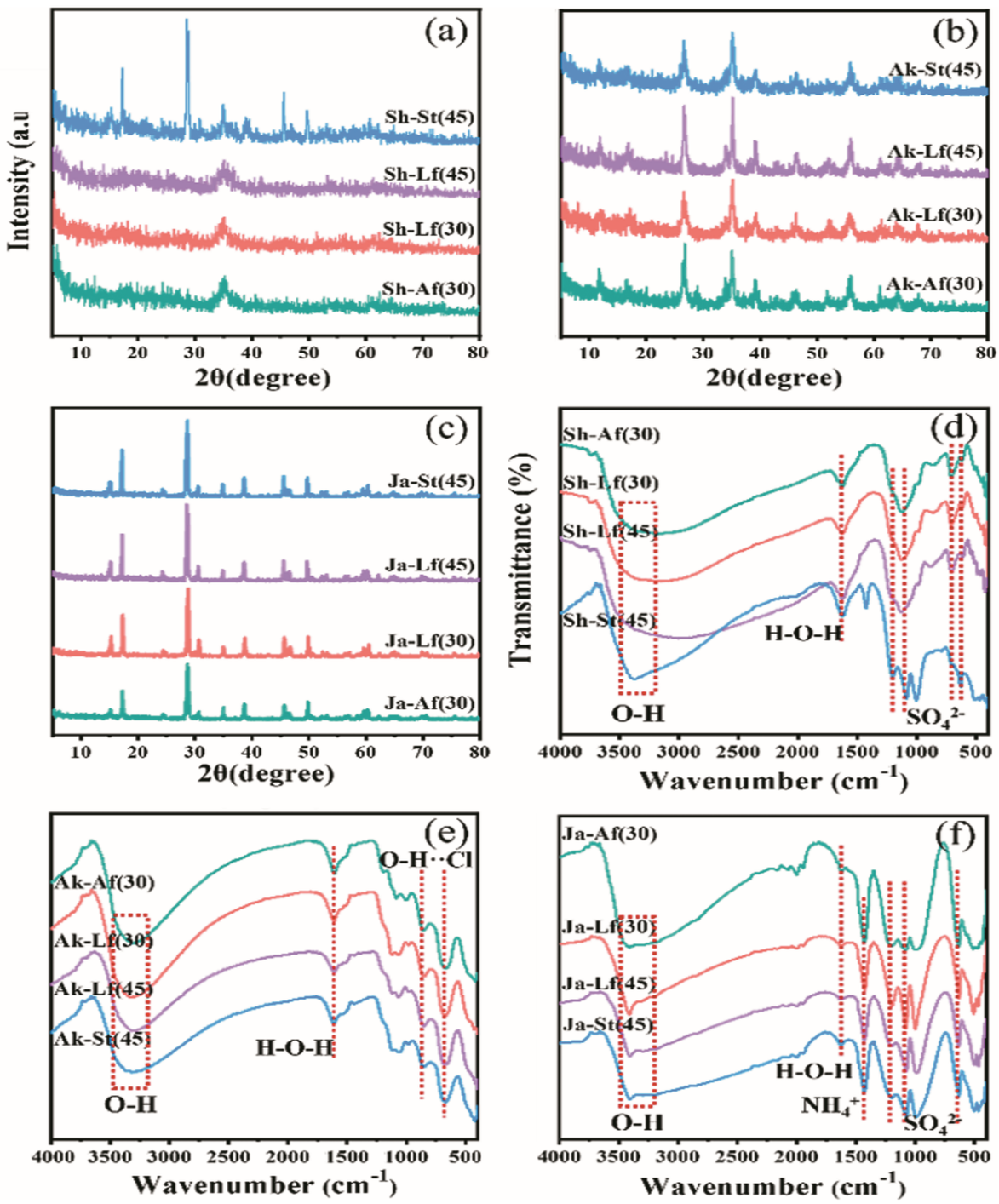


**Figure 2** XRD patterns (a, b, c) and FTIR spectra of the precipitates, of the precipitates (d, e, f)

Akaganéite formed by *S. t* (27.6 mg/g) exhibited the excellent adsorption capacity compared with *A. f* (23.4 mg/g), *L. f*(45) (24.4 mg/g), *L. f*(30) (25.3 mg/g). Moreover, compared with Sh-St(45), Sh-Lf(45) possessed better adsorption capacity owing to its weaker crystallinity. These results indicated that the difference of Cr(VI) adsorption capacity is related to the composition, morphology, size, structure, and crystallinity disparity of the minerals, and initially, it may be influenced by the biosynthesizing subject the bacteria.

### 3.3 Cr(VI) adsorption kinetic of biosynthesized Iron-minerals

Schwertmannite, Akaganéite and Ammoniojarosite formed by *A. ferrooxidans* were used to investigate adsorption kinetics and mechanism. As can be seen from Figure 4, among

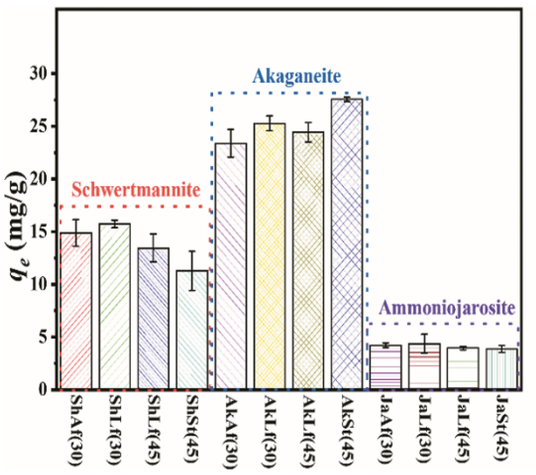


**Figure 3** Adsorption capacity ($q_e$) of the biosynthesized iron minerals by different bacteria

three types of material, Ammoniojarosite reached the adsorption equilibrium first, and its initial sorption rate of 0.696 was the lowest among these materials. As for the other two types of material, the removal efficiency was 25.0% and 32.9% for Schwertmannite and Akaganéite after 5 min adsorption, while removal efficiency of 64.9% and 85.6% was obtained after 60 min adsorption, respectively. Moreover, the initial sorption rate reached 0.972 and 1.26 for Schwertmannite and Akaganéite, respectively. The difference in Cr(VI) adsorption kinetics among the three materials may be attributed to their crystal structure. Ammoniojarosite is known to exit hexagonal, pseudo-cubic structure with no tunnel structure [19, 36]. Thus, we propose that Cr(VI) adsorption occurred on the surface sites which leads to the fast adsorption equilibrium and relatively low adsorption capacity, which is consistent with its tunnel structure and elemental composition. However, the adsorption equilibrium of Cr(VI) on Schwertmannite and Akaganéite is on the order of hours, indicating an alternative adsorption mechanism or formation of a novel chemical bond between the Cr(VI) species and adsorption surface and tunnel structures [37].

The internal micro-porous process of adsorbate diffusion into adsorbent porous takes time, and the intra-particle diffusion model can be applied to further explain the assumption [16, 38, 39]. According to the intra-diffusion particle model in Table 1, the order of adsorption rate was $K_{i1}>K_{i2}$. At the beginning, Cr(VI) was adsorbed by the exterior surface of the materials, and the first stage was the instantaneous diffusion period ($k_{i1}$). When exterior surface reached saturation, the heavy metal ions

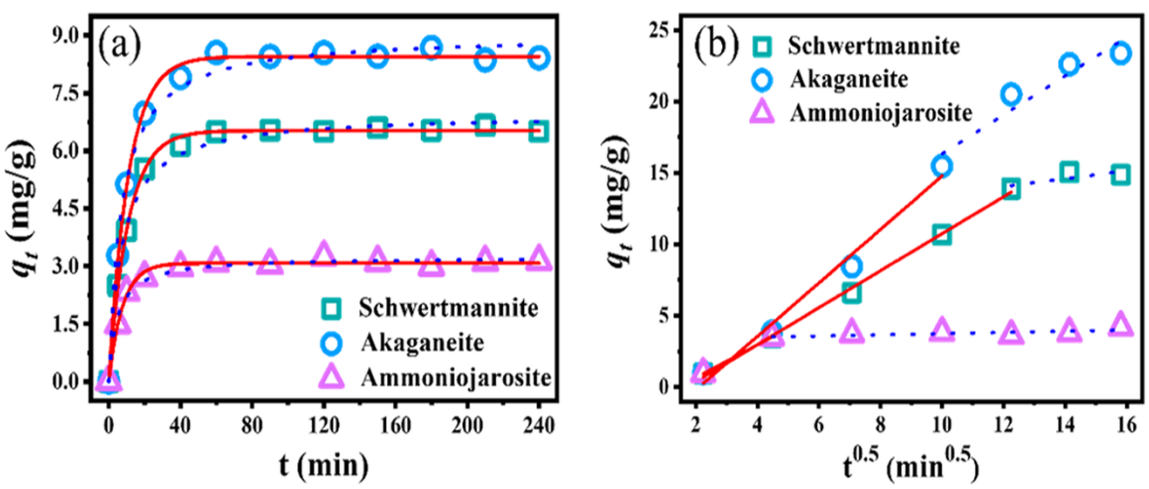


**Figure 4** Kinetics of Cr(VI) removal by biogenic Schwertmannnite, Akaganéite and Ammoniojarosite

**Table 1** Kinetics constants of each material at 50 mg/L Cr(VI)

| | Pseudo first-order rate equation | | | Pseudo second-order-rate equation | | | Intraparticle diffusion model | | | |
|---|---|---|---|---|---|---|---|---|---|---|
| | $k_1$ | $q_e$ | $R^2$ | h | $q_e$ | $R^2$ | $K_{L1}$ | $R_1^2$ | $K_{L2}$ | $R_1^2$ |
| Schwertmannite | 0.0931 | 6.53 | 0.998 | 0.972 | 6.97 | 0.988 | 1.30 | 0.997 | 0.278 | 0.285 |
| Akaganéit | 0.0920 | 8.45 | 0.997 | 1.26 | 9.02 | 0.988 | 1.87 | 0.974 | 1.36 | 0.877 |
| Ammoniojarosite | 0.131 | 3.08 | 0.991 | 0.696 | 3.24 | 0.987 | 1.14 | / | 0.0426 | 0.440 |

entered into the mesopores on the second stage. With Cr(VI) diffusing into the pores, the diffusion resistance increased, resulting in the decrease of diffusion rates ($k_{i2}$). The intra-particle diffusion rate constant of Akaganéite and Schwertmannite on second stage was 1.362 and 0.279 mg/(g·min$^{0.5}$) respectively, while the constant of Ammoniojarosite was only 0.0430 mg/(g·min$^{0.5}$), which illustrated the adsorption on second stage not significant [40]. This suggests that the deficiency of tunnel structures determined inferior adsorption capacity of Ammoniojarosite.

### 3.4 Cr(VI) adsorption isotherm of biosynthesized Iron-minerals

It was clearly seen from Figure 5 that the values of *qe* of three materials became significantly larger with increased Cr(VI) concentration and then nearly reached the platform. Among them, Ammoniojarosite and Schwertmannite reached the platform at the Cr(VI) concentration of 31.5 and 124.7 mg/L, respectively, and the increase of qe values of Akaganéite nearly reached the platform until the Cr(VI) concentration of 133.1 mg/L. Moreover, the order of three materials' best Cr(VI) adsorption capacity is Akaganéite > Schwertmannite > Ammoniojarosite. Then, the batch experimental data were fitted by the Langmuir and Freundlich isotherm models, which were represented mathematically. Table 2 presents the parameters of the Langmuir and Freudlich isotherm. Three materials' Cr(VI) adsorption process is satisfactory for the Langmuir isotherm, with all correlation coefficients ($R^2$) being over 0.97. The description of Freudlich isotherm on Schwertmannite is relatively poor ($R^2$=0.842) but well with other materials ($R^2$=0.975). Thus, it is clear that Langmuir isotherm better described the adsorption process of Schwertmannite and both models fit well with Akaganéite and Ammoniojarosite, and all the fitting curves meet the detection data's expectations. The magnitude of the Freundlich coefficient 1/n is an index of the favorability of the adsorption reaction [41], and the value of $1/n<1.0$ generally represents an advantageous adsorption condition [42]. The corresponding values of the three types of materials are 0.350, 0.333 and 0.113, which indicate favorable Cr(VI) adsorption occurred for all three materials. The fractional value of $1/n$ is assigned due to the heterogeneous nature of the adsorbent surface. Moreover, the maximal adsorption capacity of Akaganéite, Schwertmannite and Ammoniojarosite was 26.6, 17.5 and 3.90 mg/g, respectively, exceeding many iron minerals as shown in Table 3, especially Akaganéite.

The Langmuir isotherm equation and the Freundlich equation both represent different adsorption forms. The former simulates monolayer

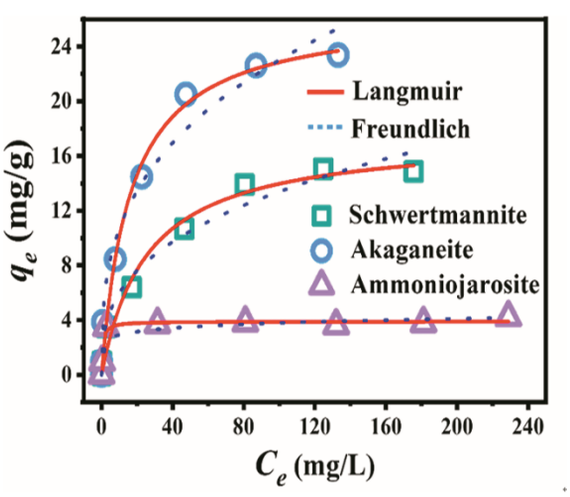


**Figure 5** Langmuir and Freundlich non-linear plots of adsorption isotherms for Cr(VI) on Schwertmannnite, Akaganéite and Ammoniojarosite

**Table 2** Langmuir and Freundlich isotherm parameters for Cr(VI) adsorption on Schwertmannnite, Akaganéite and Ammoniojarosite

| | Langmuir | | | Freundlich | | |
|---|---|---|---|---|---|---|
| | $q_m$ (mg/g) | $K_L$ | $R^2$ | $K_F$ | 1/n | $R^2$ |
| Schwertmannite | 17.5 | 0.0392 | 0.975 | 2.67 | 0.350 | 0.842 |
| Akaganéit | 26.6 | 0.0612 | 0.981 | 4.96 | 0.333 | 0.975 |
| Ammoniojarosite | 3.90 | 1.63 | 0.973 | 2.26 | 0.113 | 0.975 |

**Table 3** Comparison of Cr(VI) adsorption capacity of various adsorbents with iron-secondary minerals

| Adsorbent | $q_{max}$/(mg·g$^{-1}$) | Reference |
|---|---|---|
| Magnetic goethite | 4.32 | [53] |
| Iron oxide nanoparticles | 9.02 | [54] |
| Hematite | 2.30 | [55] |
| Goethite | 1.96 | [55] |
| Ferrihydrite | 13.0 | [56] |
| Akaganéite | 26.6 | This study |
| Schwertmannite | 17.5 | This study |
| Ammoniojarosite | 3.90 | This study |

adsorption of adsorbate onto a homogeneous adsorbing surface without lateral interaction between adsorbed molecules, and the latter postulates a multilayer adsorption process onto heterogeneous adsorption sites [43]. Therefore, their fitting results suggest that the adsorption capacities of Akaganéite, Schwertmannite and Ammoniojarosite are determined by their composition as analyzed above and highly related to their crystal structures. Both Akaganéite and Schwertmannite have well-organized tunnel structures [44], allowing chromium to penetrate through the tunnel structure and facilitate the adsorption process with enhanced adsorption capacity. Correspondingly, the poor adsorption performance of Ammoniojarosite was due to its highly crystalline, cubic shape, low specific surface binding area and non-tunnel structure. Based on the analysis above, we can conclude that molecular structure is the primary determining factor for adsorption performance.

### 3.5 Adsorption mechanism of Cr(VI) on biosynthesized Iron-minerals

The XPS spectra of S2p and Cr2p in Figure S3 AB show that $SO_4^{2-}$ was the sulfur component in the three minerals, and the valence state of chromate had not changed after adsorbed to minerals. In addition, the atomic concentration (% ) of Cr on Ammoniojarosite surface area was the highest, which is completely opposite to its adsorption capacity. According to the XPS spectra of Fe2p, the atomic concentration (% ) of Fe on the material surfaces reached 16.8%, 12.6% and 9.73% in Akaganéite, Schwertmannite and Ammoniojarosite respectively (Figure S3(c), Table S2). Moreover, their Cr(VI) adsorption capacity (Table 2) was consistent with the Fe atomic concentration. Therefore we hypothesized that Fe plays a critical role in Cr(VI) removal through processes such as adsorption [45, 46]. Although all materials had considerable surface carbon content, Ammoniojarosite in particular had the highest, suggesting that bacteria absorbed on the mineral surface and mediated the formation process (Figure S3(d)). Since extracellular polymeric substances or metabolites of bacteria may play a critical role in material nucleation, grading and growth, biosynthesized materials would be varied when different bacteria are involved.

The FTIR spectra of minerals of minerals before and after adsorption of Cr(VI) are shown in Figure 2. The intense absorption observed in the region 3000 to 3400 $cm^{-1}$ can be attributed to O—H stretching, which were present in all of the twelve samples and is important for the stability of iron oxyhydroxides and subsequent adsorption process. The band observed around 1610 $cm^{-1}$ indicates H—O—H deformation. Other peaks existed in Schwertmannite and Ammoniojarosite including bands at 1200, 1070 $cm^{-1}$ and 630, 680 $cm^{-1}$ are due to $v_3$ and $v_4$ vibration mode of the sulfate [47-49]. Note that sulfate peak transmissivity of sample Sh-St (45) was only 20%, which indicate the lower sulfate content in Sh-St(45) that could lead to the formation of cubic in the precipitate. The bands around 850 and 670 $cm^{-1}$ are vibration modes of the two O—H···Cl hydrogen bonds present, which are characteristic of chloride containing Akaganéite [9]. An obvious adsorption band around 1429 $cm^{-1}$ was observed in sample Ammoniojarosite, confirming the presence of $NH_4^+$ . However, the band intensity of O—H, sulfate and O—H···Cl of both materials (Figure S4) with tunnel structure obviously reduced after adsorption of Cr(VI), this is the direct evidence that the adsorption occurred through a combination of surface complexation with active hydroxyl groups, exchange with both surface adsorbed, structural sulfate sites and O—H···Cl sites. These results suggest that the mechanism of Cr(VI) adsorption on these materials involves ligand exchange, similar to the arsenic adsorption mechanism on Schwertmannite and Akaganéite [11, 37].

To further verify the above speculation, XAFS was used for in-depth analysis. XAFS analysis of Cr showed that there were obvious Cr(VI)-O covalent bonds on the surfaces of three minerals after adsorption (Figures 6(a) and (b)), which may be due to the adsorption of chromate on the mineral surface consistent with the XPS data of Cr2p or may be formed by the combination of chromate and O—H on the mineral surface according to the FTIR spectra. In addition, the XAFS analysis of Fe in minerals also be explored. The data in k-space and R-space prove that the adsorption of Cr(VI) has no effect on minerals about the formation of new covalent bonds and the disappearance of the original covalent bonds (Figures 6(c) and (d)), indicating

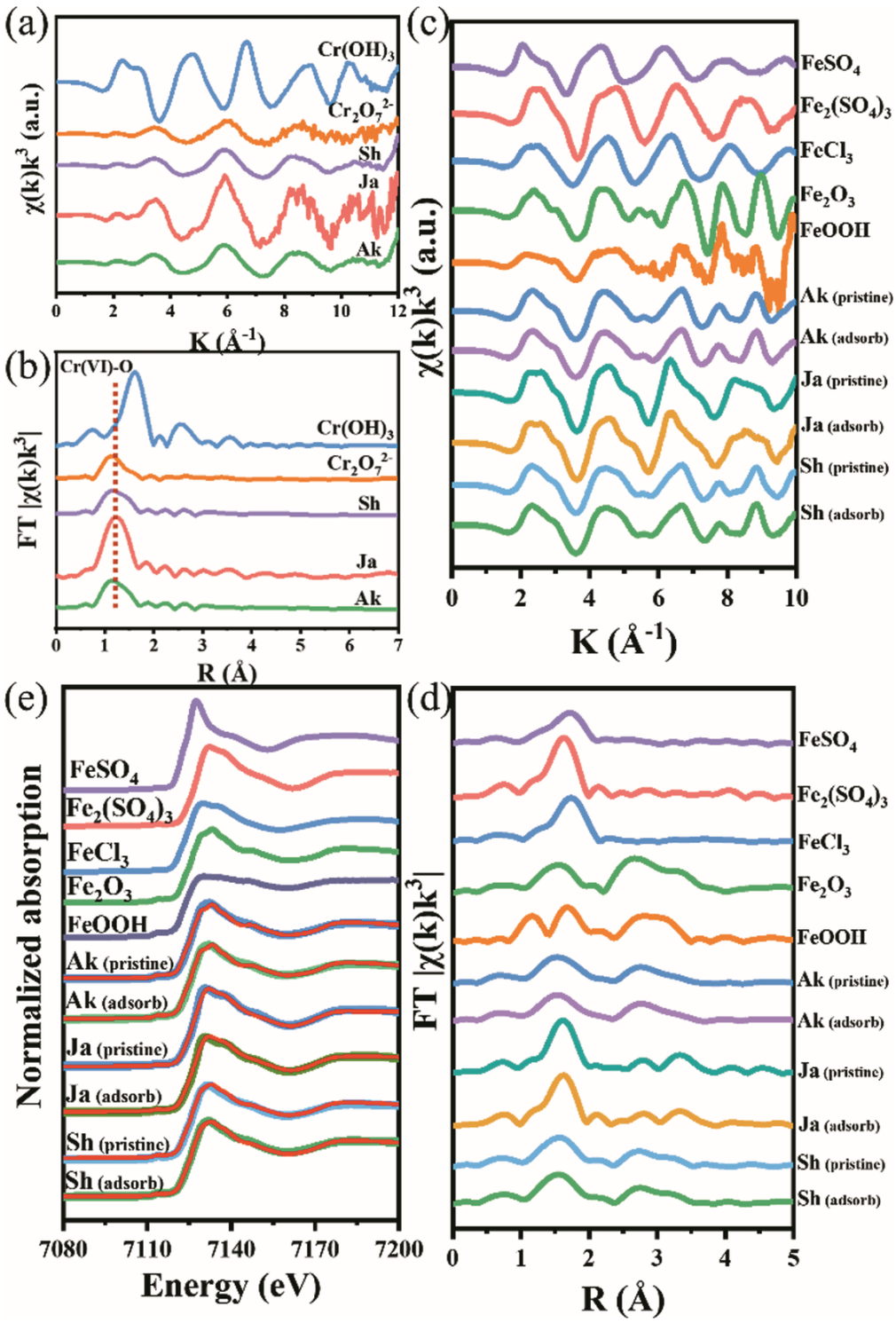


**Figure 6** k3 -weighted chi spectra (a) and Fourier-transformed real part (b) of Cr; k3 -weighted chi spectra (c) and Fourier-transformed real part (d) of Fe; Fe K-edge XANES spectra of minerals (blue line), best fit (red line), and reference standards (e). Abbreviations: Ak=Akaganéite, Ja=Ammoniojarosite, Sh=Schwertmannite, Ak (pristine) = primitive Akaganéite, Ak (adsorb)=Akaganéite adsorbed with Cr(VI)

that the adsorption pathways without the destruction of mineral structure, such as electrostatic adsorption and ligand exchange, were the main contributors to the adsorption of Cr(VI) [50-52]. Moreover, the components of iron minerals before and after adsorption were also analyzed (Figure 6(e), Table 4). Akaganéite has Fe(III)-O (99.6%) and Fe (III) -Cl (0.6%), while the adsorption of Cr(VI)

**Table 4** The components (%) of iron minerals before and after adsorption

| | | $FeCl_3$ | $Fe_2O_3$ | $FeSO_4$ | $Fe_2(SO_4)_3$ | FeOOH |
|---|---|---|---|---|---|---|
| Akaganéit | Pristine | 0.600 | 99.4 | — | — | — |
| | Adsorb | 0 | 100 | — | — | — |
| Ammoniojarosite | Pristine | — | — | 15.0 | 85.0 | — |
| | Adsorb | — | 6.90 | 9.30 | 70.9 | 12.9 |
| Schwertmannite | Pristine | — | 51.5 | 11.0 | 37.4 | — |
| | Adsorb | — | 56.2 | 6.20 | 30.3 | 7.30 |

Pristine: Primitive mineral, adsorb: mineral adsorbed with Cr(VI)

makes the Fe(III) -Cl disappears completely, indicating that the O—H·Cl sites in Akaganéite may be replaced by chromate. Fe-$SO_4^{2-}$ is the Fe-components of Ammoniojarosite, which will partly change to Fe(III) -O (6.90%) and Fe-OH (12.9%) after adsorption of Cr(VI), demonstrating that $SO_4^{2-}$ in Ammoniojarosite was partially replaced, moreover, the mineral was partly dissolved and re-precipitated to form FeOOH. Similar changes have also been discovered in the system of adsorption of Cr(VI) by Schwertmannite. The Fe-$SO_4^{2-}$ in Schwertmannite decreased from 48.4% to 36.5%, while Fe(III)-O and Fe-OH increased from 51.5%, 0 to 56.2%, 7.30%, respectively. These results indicate that the replacement of $SO_4^{2-}$ with $CrO_4^{2-}$, the dissolution and reprecipitation of the minerals also occur in the system of adsorption of Cr(VI) by Schwertmannite.

Based on the above results, the schematic illustration of the Cr(VI) adsorption mechanism by Ammoniojarosite, Akaganéite, and Schwertmannite is shown in Figure 7. The tunnel free crystal structure of Ammoniojarosite makes its adsorption of Cr(VI) only have one stage, which occurs in the early stage of the reaction. On the surface of Ammoniojarosite, the hydrogen bonding between Cr (VI) and O—H, the electrostatic interaction between Cr(VI) and mineral, and the ligand exchange between $CrO_4^{2-}$ and $SO_4^{2-}$ were contributed to the adsorption of Cr(VI). The tunnel structure of Akaganéite brings two stages of Cr(VI) adsorption: on the surface of Akaganéite, hydrogen bonding, electrostatic interaction, and ligand exchange between $CrO_4^{2-}$ and O—H·Cl leads to the adsorption of Cr(VI), and then, Cr(VI) will enter into the mesopores for new adsorption when exterior surface reached saturation. Owing to the tunnel structure similar to that of Akaganéite, Schwertmannite also have two stages of adsorption of Cr(VI) on the mineral surface and mesopores through hydrogen bonding, electrostatic interaction, and ligand exchange between $CrO_4^{2-}$ and $SO_4^{2-}$.

## 4 Conclusion

In this study, Schwertmannite, Akaganéite, and Ammoniojarosite were biosynthesized by different bacteria and employed to remove Cr(VI). The results of SEM-EDS, FTIR, and XRD showed that bacteria are critical in mediating the mineral formation process: the morphology, crystallinity, grain size and specific surface area of each mineral varied upon different bacteria and culturing conditions. Different biosynthetic minerals exhibit diverse Cr(VI) adsorption capacities. The adsorption of Cr(VI) onto three minerals followed the Pseudo 1 st order and pseudo 2nd order and the Langmuir and Freundlich isotherm models. The maximum adsorption capacities of Cr(VI) by Schwertmannite, Akaganéite, and Ammoniojarosite are 17.5, 26.6, and 3.90 mg/g respectively. Results of XPS, FTIR, and XAFS suggest that Cr(VI) adsorption on iron-minerals involves hydrogen bonding, electrostatic interaction, and ligand exchange. The adsorption only occurred on the surface of Ammoniojarosite, while for Akaganéite and Schwertmannite, the tunnel structure greatly facilitated the adsorption process and improved adsorption capacity. This work makes a theoretical foundation for selecting suitable chromium removal reagents and selecting suitable biosynthetic microorganisms according to different environmental conditions.

## Contributors

The overarching research goals were developed by GAN Min and ZHU Jianyu. ZHANG

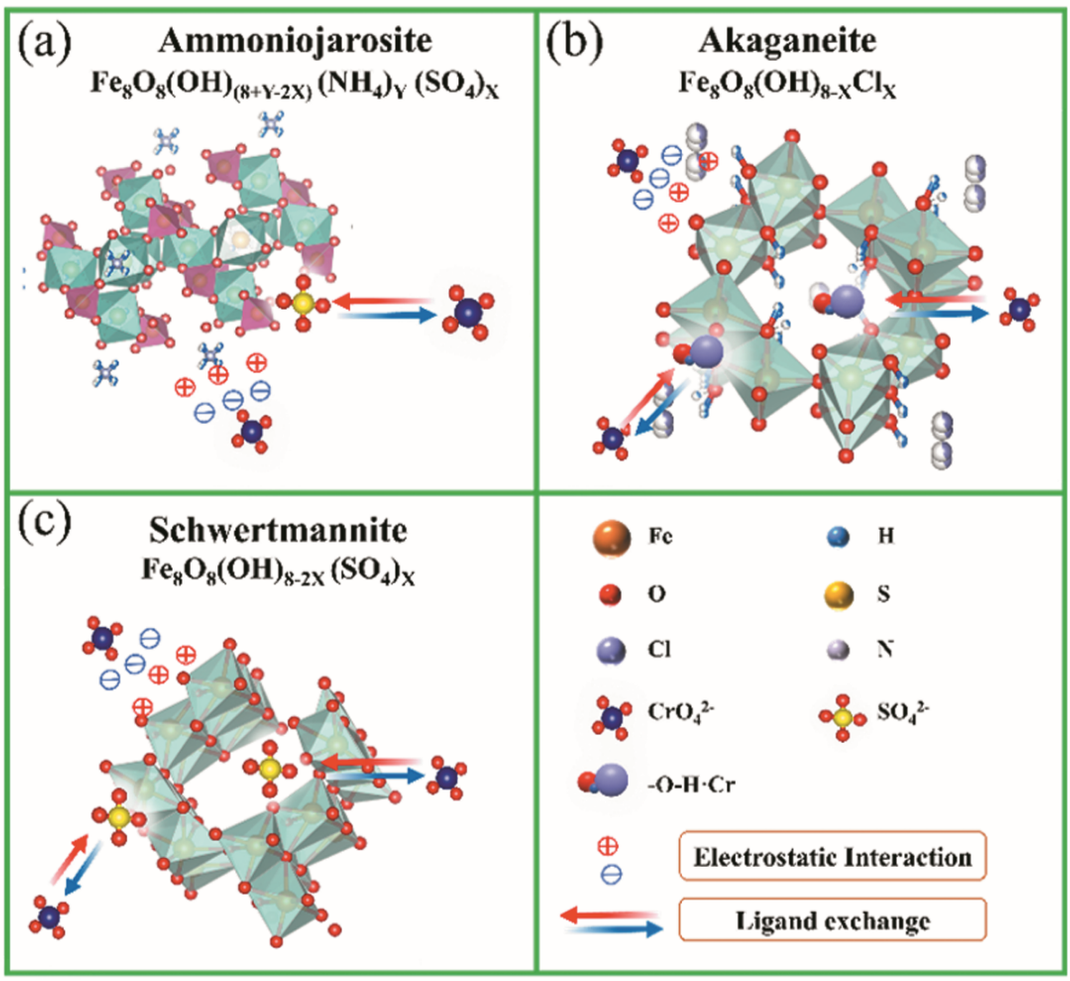


**Figure 7** Schematic illustration of the Cr(VI) adsorption mechanism by Ammoniojarosite (a), Akaganéite (b), and Schwertmannite (c)

Ke conducted the literature review and wrote the draft and validated the proposed method with practical experiments. ZENG Xiangfeng, WANG Jun, HE Qiang, and Terry C. Hazen analyzed the experimental data. ZHANG Ke edited the draft of the manuscript. LIU Junwu and FANG Yingchun edited the draft of manuscript. All authors replied to reviewers' comments and revised the final version.

## Supplementary materials

https://qr.csupress.com.cn/Public/ResourceList/Detail/56902
Please scan the QR code or visit the URL link to get the supporting information

## Conflict of interest

ZHANG Ke, ZENG Xiang-feng, WANG Jun, GAN Min, ZHU Jian-yu, HE Qiang, Terry C. Hazen3, LIU Jun-wu, FANG Ying-chun declare that they have no conflict of interest.

## Reference

[1] AO Ming, CHEN Xiao-ting, DENG T, et al. Chromium biogeochemical behaviour in soil-plant systems and remediation strategies: A critical review [J]. Journal of Hazardous Materials, 2022, 424(Pt A): 127233. DOI:10.1016/j.jhazmat.2021.127233.

[2] VAIOPOULOU E, GIKAS P. Regulations for chromium emissions to the aquatic environment in Europe and elsewhere [J]. Chemosphere, 2020, 254: 126876. DOI: 10.1016/j.chemosphere.2020.126876.

[3] UKHUREBOR K E, AIGBE U O, ONYANCHA R B, et al. Effect of hexavalent chromium on the environment and removal techniques: A review [J]. Journal of Environmental Management, 2021, 280: 111809. DOI: 10.1016/j.

jenvman.2020.111809.

[4] ISLAM M A, ANGOVE M J, MORTON D W, et al. A mechanistic approach of chromium (VI) adsorption onto manganese oxides and boehmite [J]. Journal of Environmental Chemical Engineering, 2020, 8(2): 103515. DOI:10.1016/j.jece.2019.103515.

[5] AIGBE U O, OSIBOTE O A. A review of hexavalent chromium removal from aqueous solutions by sorption technique using nanomaterials [J]. Journal of Environmental Chemical Engineering, 2020, 8(6): 104503. DOI: 10.1016/j.jece.2020.104503.

[6] ZHU Chang, WANG Qian, HUANG Xiao-xiao, et al. Microscopic understanding about adsorption and transport of different Cr(VI) species at mineral interfaces [J]. Journal of Hazardous Materials, 2021, 414: 125485. DOI: 10.1016/j.jhazmat.2021.125485.

[7] ZHU Jian-yu, CHEN Fang, GAN Min. Controllable biosynthesis of nanoscale schwertmannite and the application in heavy metal effective removal [J]. Applied Surface Science, 2020, 529: 147012. DOI: 10.1016/j.apsusc.2020.147012.

[8] CHEN Gong-ning, SHAH K J, SHI Lin, et al. Removal of Cd (II) and Pb(II) ions from aqueous solutions by synthetic mineral adsorbent: Performance and mechanisms [J]. Applied Surface Science, 2017, 409: 296−305. DOI:10.1016/j.apsusc.2017.03.022.

[9] XIONG Hui-xin, LIAO Yue-hua, ZHOU Li-xiang, et al. Biosynthesis of nanocrystal akaganéite from $FeCl_2$ solution oxidized by *Acidithiobacillus ferrooxidans* cells [J]. Environmental Science & Technology, 2008, 42(11): 4165−4169. DOI:10.1021/es702933v.

[10] REGENSPURG S, PEIFFER S. Arsenate and chromate incorporation in schwertmannite [J]. Applied Geochemistry, 2005, 20(6): 1226 − 1239. DOI: 10.1016/j.apgeochem.2004.12.002.

[11] BURTON E D, BUSH R T, JOHNSTON S G, et al. Sorption of arsenic(V) and arsenic(III) to schwertmannite [J]. Environmental Science & Technology, 2009, 43(24): 9202−9207. DOI:10.1021/es902461x.

[12] SCHOEPFER V A, BURTON E D. Schwertmannite: A review of its occurrence, formation, structure, stability and interactions with oxyanions [J]. Earth-Science Reviews, 2021, 221: 103811. DOI:10.1016/j.earscirev.2021.103811.

[13] GAN Min, SUN Sheng-jie, ZHENG Zhi-he, et al. Adsorption of Cr(VI) and Cu(II) by $AlPO_4$ modified biosynthetic schwertmannite [J]. Applied Surface Science, 2015, 356: 986−997. DOI:10.1016/j.apsusc.2015.08.200.

[14] BOILY J F, GASSMAN P L, PERETYAZHKO T, et al. FTIR spectral components of schwertmannite [J]. Environmental Science & Technology, 2010, 44(4): 1185 − 1190. DOI: 10.1021/es902803u.

[15] VILLALBA J C, BEREZOSKI S, DE ALMEIDA CAVICCHIOLLI K, et al. Structural refinement and morphology of synthetic akaganèite crystals, [β -FeO(OH) [J]. Materials Letters, 2013, 104: 17 − 20. DOI: 10.1016/j.matlet.2013.04.004.

[16] LAZARIDIS N K, BAKOYANNAKIS D N, DELIYANNI E A. Chromium(VI) sorptive removal from aqueous solutions by nanocrystalline akaganèite [J]. Chemosphere, 2005, 58(1): 65−73. DOI:10.1016/j.chemosphere.2004.09.007.

[17] DELIYANNI E A, BAKOYANNAKIS D N, ZOUBOULIS A I, et al. Sorption of As(V) ions by akaganéite-type nanocrystals [J]. Chemosphere, 2003, 50(1): 155−163. DOI: 10.1016/S0045-6535(02)00351-X.

[18] ZHANG Duo-rui, XIA Jin-lan, NIE Zhen-yuan, et al. Mechanism by which ferric iron promotes the bioleaching of arsenopyrite by the moderate thermophile Sulfobacillus thermosulfidooxidans [J]. Process Biochemistry, 2019, 81: 11−21. DOI:10.1016/j.procbio.2019.03.004.

[19] BASCIANO L C, PETERSON R C. The crystal structure of ammoniojarosite, $(NH_4)Fe_3(SO_4)_W(OH)_6$ and the crystal chemistry of the ammoniojarosite – hydronium jarosite solid-solution series [J]. Mineralogical Magazine, 2007, 71(4): 427−441. DOI:10.1180/minmag.2007.071.4.427.

[20] JIN De-cheng, WANG Xiao-meng, LIU Lan-lan, et al. A novel approach for treating acid mine drainage through forming schwertmannite driven by a mixed culture of Acidiphilium multivorum and *Acidithiobacillus ferrooxidans* prior to lime neutralization [J]. Journal of Hazardous Materials, 2020, 400: 123108. DOI: 10.1016/j.jhazmat.2020.123108.

[21] KARIMIAN N, JOHNSTON S G, BURTON E D. Iron and sulfur cycling in acid sulfate soil wetlands under dynamic redox conditions: A review [J]. Chemosphere, 2018, 197: 803−816. DOI:10.1016/j.chemosphere.2018.01.096.

[22] SCHWERTMANN U, CARLSON L. The pH-dependent transformation of schwertmannite to goethite at 25℃ [J]. Clay Minerals, 2005, 40(1): 63 − 66. DOI: 10.1180/0009855054010155.

[23] MIYATA N, TAKAHASHI A, FUJII T, et al. Biosynthesis of schwertmannite and goethite in a bioreactor with acidophilic Fe(II) -oxidizing betaproteobacterium strain GJ-E10 [J]. Minerals, 2018, 8(3): 98. DOI:10.3390/min8030098.

[24] ZHANG Yu-yang, ZHU Zi-ying, LIAO Yan-guang, et al. Effects of Fe(II) source on the formation and reduction rate of biosynthetic mackinawite: Biosynthesis process and removal of Cr(VI) [J]. Chemical Engineering Journal, 2021, 421: 129723. DOI:10.1016/j.cej.2021.129723.

[25] SONG Xiao-jie, SHI Xian-yang. Biosynthesis of Ag/reduced graphene oxide nanocomposites using Shewanella oneidensis MR-1 and their antibacterial and catalytic applications [J]. Applied Surface Science, 2019, 491: 682−689. DOI:10.1016/j.apsusc.2019.06.154.

[26] HARNEIT K, GÖKSEL A, KOCK D, et al. Adhesion to metal sulfide surfaces by cells of *Acidithiobacillus ferrooxidans*, Acidithiobacillus thiooxidans and Leptospirillum ferrooxidans [J]. Hydrometallurgy, 2006, 83(1−4): 245−254. DOI:10.1016/j.hydromet.2006.03.044.

[27] VARDANYAN A, KHACHATRYAN A, CASTRO L, et al. Bioleaching of sulfide minerals by leptospirillum ferriphilum CC from polymetallic mine (Armenia) [J]. Minerals, 2023, 13 (2): 243. DOI:10.3390/min13020243.

[28] BOGDANOVA T I, TSAPLINA I A, KONDRAT'EVA T F, et al. Sulfobacillus thermotolerans sp. nov., a thermotolerant, chemolithotrophic bacterium [J]. International Journal of Systematic and Evolutionary Microbiology, 2006, 56(5): 1039−1042. DOI:10.1099/ijs.0.64106-0.

[29] YI Qing, WU Song-lin, SOUTHAM G, et al. Acidophilic

iron- and sulfur-oxidizing bacteria, *Acidithiobacillus ferrooxidans*, drives alkaline pH neutralization and mineral weathering in Fe ore tailings [J]. Environmental Science & Technology, 2021, 55(12): 8020 − 8034. DOI: 10.1021/acs.est.1c00848.

[30] QIN Wen, WANG Chen-yu, MA Yu-xuan, et al. Microbe-mediated extracellular and intracellular mineralization: Environmental, industrial, and biotechnological applications [J]. Advanced Materials, 2020, 32(22): 1907833. DOI: 10.1002/adma.201907833.

[31] ZHU Jian-yu, GAN Min, ZHANG Dan, et al. The nature of Schwertmannite and Jarosite mediated by two strains of *Acidithiobacillus ferrooxidans* with different ferrous oxidation ability [J]. Materials Science and Engineering: C, 2013, 33(5): 2679−2685. DOI:10.1016/j.msec.2013.02.026.

[32] XIONG Hui-xin, GUO Rong. Effects of chloride acclimation on iron oxyhydroxides and cell morphology during cultivation of *Acidithiobacillus ferrooxidans* [J]. Environmental Science & Technology, 2011, 45(1): 235−240. DOI:10.1021/es1019146.

[33] XIONG Hui-xin, LIAO Yue-hua, ZHOU Li-xiang. Influence of chloride and sulfate on formation of akaganéite and schwertmannite through ferrous biooxidation by acidithiobacillus ferrooxidans cells [J]. Environmental Science & Technology, 2008, 42(23): 8681 − 8686. DOI: 10.1021/es801646j.

[34] BURSTEIN G T. Iron oxides in the laboratory, preparation and characterization [J]. Corrosion Science, 1992, 33(7): 1189. DOI:10.1016/0010-938x(92)90174-2.

[35] BISHOP J L, MURAD E, DYAR M D. Akaganeite and schwertmannite: Spectral properties and geochemical implications of their possible presence on Mars [J]. American Mineralogist, 2015, 100(4): 738−746. DOI:10.2138/am-2015-5016.

[36] SMITH W L, LAMPERT J E. Crystal data for ammoniojarosite. $NH_4Fe_3(OH)_6(SO_4)_2$ [J]. Journal of Applied Crystallography, 1973, 6(6): 490 − 491. DOI: 10.1107/s0021889873009301.

[37] LIAO Yue-hua, LIANG Jian-ru, ZHOU Li-xiang. Adsorptive removal of As(III) by biogenic schwertmannite from simulated As-contaminated groundwater [J]. Chemosphere, 2011, 83(3): 295 − 301. DOI: 10.1016/j.chemosphere.2010.12.060.

[38] WU F C, TSENG R L, JUANG R S. Initial behavior of intraparticle diffusion model used in the description of adsorption kinetics [J]. Chemical Engineering Journal, 2009, 153(1−3): 1−8. DOI:10.1016/j.cej.2009.04.042.

[39] LAZARIDIS N K, CHARALAMBOUS C. Sorptive removal of trivalent and hexavalent chromium from binary aqueous solutions by composite alginate ‑ goethite beads [J]. Water Research, 2005, 39(18): 4385 − 4396. DOI: 10.1016/j.watres.2005.09.013.

[40] ARSENIE T, CARA I G, POPESCU M C, et al. Evaluation of the adsorptive performances of rapeseed waste in the removal of toxic metal ions in aqueous media [J]. Water, 2022, 14(24): 4108. DOI:10.3390/w14244108.

[41] MALEKI S, KARIMI-JASHNI A. Optimization of Ni(II) adsorption onto Cloisite Na+ clay using response surface methodology [J]. Chemosphere, 2020, 246: 125710. DOI: 10.1016/j.chemosphere.2019.125710.

[42] TANG Wang-wang, ZENG Guang-ming, GONG Ji-lai, et al. Simultaneous adsorption of atrazine and Cu (II) from wastewater by magnetic multi-walled carbon nanotube [J]. Chemical Engineering Journal, 2012, 211: 470 − 478. DOI: 10.1016/j.cej.2012.09.102.

[43] AKEMOTO Y, SAKTI S C W, KAN M, et al. Interpretation of the interaction between cesium ion and some clay minerals based on their structural features [J]. Environmental Science and Pollution Research, 2021, 28(11): 14121−14130. DOI:10.1007/s11356-020-11476-7.

[44] SHAN Jun, HE Meng-chang, LIU Peng, et al. Antimony immobilization mechanism on schwertmannite: Insights from the microstructure of schwertmannite [J]. Geochimica et Cosmochimica Acta, 2023, 359: 71 − 83. DOI: 10.1016/j.gca.2023.09.005.

[45] JIANG Shu-qi, YAN Xin-ran, PEACOCK C L, et al. Adsorption of Cr(VI) on Al-substituted hematites and its reduction and retention in the presence of $Fe^{2+}$ under conditions similar to subsurface soil environments [J]. Journal of Hazardous Materials, 2020, 390: 122014. DOI: 10.1016/j.jhazmat.2019.122014.

[46] LI Xiao-fei, GUO Chu-ling, JIN Xiao-hu, et al. Mechanisms of Cr(VI) adsorption on schwertmannite under environmental disturbance: Changes in surface complex structures [J]. Journal of Hazardous Materials, 2021, 416: 125781. DOI: 10.1016/j.jhazmat.2021.125781.

[47] TULADHAR A, DEWAN S, KUBICKI J D, et al. Spectroscopy and ultrafast vibrational dynamics of strongly hydrogen bonded OH species at the α -$Al_2O_3(11\bar{2}0)/H_2O$ interface [J]. The Journal of Physical Chemistry C, 2016, 120 (29): 16153−16161. DOI:10.1021/acs.jpcc.5b12486.

[48] RANI M, YADAV J, SHANKER U. Green synthesis, kinetics and photoactivity of novel nickel oxide-decorated zinc hexacyanocobaltate catalyst for efficient removal of toxic Cr(VI) [J]. Journal of Environmental Chemical Engineering, 2021, 9(2): 105073. DOI: 10.1016/j.jece.2021.105073.

[49] YAO Qian, GUO Chu-ling, LI Xiao-fei, et al. Synergy of oxalic acid and sunlight triggered Cr(III) -bearing Schwertmannite transformation: Reaction mechanism, Cr and C spatial distribution and speciation on the nano scale [J]. Geochimica et Cosmochimica Acta, 2022, 329: 70 − 86. DOI:10.1016/j.gca.2022.05.018.

[50] ZHANG B, CHEN Nan, FENG Chuan-ping, et al. Adsorption for phosphate by crosslinked/non-crosslinked-chitosan-Fe(III) complex sorbents: Characteristic and mechanism [J]. Chemical Engineering Journal, 2018, 353: 361−372. DOI:10.1016/j.cej.2018.07.092.

[51] HE Jiao-jie, XU Yu-hong, WANG Wei, et al. Ce(III) nanocomposites by partial thermal decomposition of Ce-MOF for effective phosphate adsorption in a wide pH range [J]. Chemical Engineering Journal, 2020, 379: 122431. DOI: 10.1016/j.cej.2019.122431.

[52] NAGOYA S, NAKAMICHI S, KAWASE Y. Mechanisms of phosphate removal from aqueous solution by zero-valent iron: A novel kinetic model for electrostatic adsorption, surface complexation and precipitation of phosphate under oxic conditions [J]. Separation and Purification Technology,

2019, 218: 120−129. DOI:10.1016/j.seppur.2019.02.042.
[53] LIU Zhan-meng, CHEN Gang, XU Li-chun, et al. Removal of Cr(VI) from wastewater by a novel adsorbent of magnetic goethite: Adsorption performance and adsorbent characterisation [J]. ChemistrySelect, 2019, 4(47): 13817−13827. DOI:10.1002/slct.201904125.
[54] SINGH P N, TIWARY D, SINHA I. Improved removal of Cr (VI) by starch functionalized iron oxide nanoparticles [J]. Journal of Environmental Chemical Engineering, 2014, 2(4): 2252−2258. DOI:10.1016/j.jece.2014.10.003.
[55] AJOUYED O, HUREL C, AMMARI M, et al. Sorption of Cr (VI) onto natural iron and aluminum (oxy)hydroxides: Effects of pH, ionic strength and initial concentration [J]. Journal of Hazardous Materials, 2010, 174(1−3): 616−622. DOI:10.1016/j.jhazmat.2009.09.096.
[56] NI Chun-yan, LIU Shan, CUI Lin-jing, et al. Adsorption performance of Cr(vi) onto Al-free and Al-substituted ferrihydrites [J]. RSC Advances, 2016, 6(71): 66412−66419. DOI:10.1039/c6ra09465a.

**(Edited by HE Yun-bin)**

## 中文导读

### 生物成因铁基矿物的Cr(VI)吸附机制对比探究

**摘要：**施氏矿物、四方纤铁矿和铵黄铁钒是常见的可由生物成矿的铁基次生矿物，在水体污染治理领域具有极大地应用潜力。因此，深入阐明其生物成矿机制及重金属吸附机制，理解其在环境中的异质性，对于这三种矿物的实际应用具有重要意义。本文探究了四种典型嗜酸微生物(*A. ferrooxidans*, *L. ferrooxidans*, *L. ferriphilum* YSK 和 *S, thermosulfidooxidans*)对三种铁基次生矿物生物成矿过程的特征，表征了其精细矿物学性质并解析了其重金属吸附机制。结果显示，微生物种类与溶液化学组分均可以影响矿物的元素组成、基团差异、形态、结晶度、粒度和比表面积等性质，进而显著影响矿物的吸附性能。生物成矿的四方纤铁矿、施氏矿物和铵黄铁钒具有显著不同的Cr(VI)吸附能力，最大吸附量分别为26.59 mg/g、17.53 mg/g和3.90 mg/g。此外，在具体吸附机制方面，三种铁基矿物主要通过氢键、静电相互作用和配体交换吸附Cr(VI)。其中，铵黄铁钒主要为表面吸附，而四方纤铁矿与施氏矿物不仅可以在矿物表面吸附Cr(VI)，还可以通过隧道结构进行吸附，进而具备更高的Cr(VI)吸附性能。本文的研究结果为具有高吸附容量的生物成因矿物的开发与实际应用提供了理论基础。

**关键词：**铁基次生矿物；生物合成；生物矿化；Cr(VI)吸附；重金属去除矿物